www.vbripress.com/aml, DOI:10.5185/amlett.2016.6394 Published online by the VBRI Press in 2016

Chromium (VI) ions adsorption onto barium hexaferrite magnetic nano-adsorbent

Aida Mohammadi, Abolghasem Ataie, Saeed Sheibani*

School of Metallurgy and Materials Engineering, College of Engineering, University of Tehran, Tehran, Iran

*Corresponding author. Tel: (+98) 82084068; Fax: (+98) 21-88006076; E-mail: ssheibani@ut.ac.ir

Received: 31 December 2015, Revised: 09 February 2016 and Accepted: 20 May 2016

ABSTRACT

Barium hexaferrite ($BaFe_{12}O_{19}$) magnetic nano-powder was prepared by co-precipitation method. The effectiveness of different chemical synthesis variables such as solvent and mechanical milling on the adsorption efficiency of barium hexaferrite nano-particles to remove Cr (VI) ions from aqueous solutions was examined. Structural, magnetic, and adsorption properties of the powders are investigated by different techniques. X-ray diffraction analysis revealed that barium hexaferrite formed at a relatively low temperature of 700˚C in the sample prepared with a mixture of water/alcohol as a solvent. The FESEM and VSM studies confirmed that all samples had a plate like structure with a particle size in the range of 87-145 nm and high magnetic properties. It was demonstrated that nanometer barium hexaferrite was produced to be an operative adsorbent for removal of Cr (VI) ions from solutions. Different Cr (VI) adsorption experiments were carried out by controlling effective adsorption factors. It was revealed that the sample calcined at a temperature of 700°C and then milled for 5 h (owing themaximum surface area 13 m^2/g) showed the highest removal efficiency of 99.5% at pH 3.0, amount of nano adsorbent 1.5 g, initial chromium concentration 133 mg/l, and contact time 1 h. FTIR analysis showed that due to the existence of Cr-O stretching band on the surface of nano-particles, the electrostatic reaction between Cr (VI) ions and nano-adsorbent is possible. The adsorption data were best fitted with the pseudo-second-order kinetic model. Also, the equilibrium adsorption capacity of Cr (VI) calculated from adsorption experiments was found to be 13.25 mg/g. Adsorption studies indicated that the potential use of barium hexaferrite nano-adsorbents for the removal of the other heavy metal ions without sacrificing adsorption capacity can be practical.

Keywords: Barium hexaferrite; nano-adsorbent; adsorption; Cr (VI) ions; kinetics.

Introduction

It is important to develop new techniques for the treatment of natural water supplies and industrial wastewater polluted by heavy metal ions. In most of all industry there are non-environmentally friendly chemicals in the effluents. In particular, environmental contamination by Cr (VI) widely used in alloy and steel manufacturing, electroplating, metal finishing, leather tanning, dying, and photography industries is a major problem in industrial areas **[1]**. It is reported that the effluents from these industries often contain around 50-100 mg/L of Cr (VI), which are above 1000 times higher than the maximum allowed concentration of standard for the wastewater discharge **[1]**. In addition, Cr (VI) is very toxic to living organisms resulting in severe health problems such as pulmonary congestion and skin irritation **[2]**. So, in light of Cr toxicity and environmental hazards, there is a need to remove this metallic element but also to recycle and use again it, which is beneficial an economical point of view.

Today a variety of methods have been build up to remove Cr (VI) compounds from industrial wastewater. A few worth to mention are chemical precipitation, ion exchange, chemical coagulation and flocculation, solvent extraction, electrochemical cells, filtration, and reverse osmosis **[1]**. However, most of these methods possess some shortcomings: high waste treatment equipment cost, large consumption of reagents, disposal of metal sludge, and incompetent recovery of treated metals for reprocess **[2]**. Therefore, in view of the growing concern about environmental subjects, efforts have been made to extend new techniques for removing Cr (VI) pollutant form aquatic environment. The new improvements in using adsorption process with the aid ofnano-sized magnetic particles have solved some of the problems in this regard due to their multiple and unique characteristics: high surface area, magnetic response, fast adsorption kinetics, simplicity, and high efficiency **[1]**.

Many attempts have been carried out showing the high efficiency of magnetic nano-particles in removing Cr (VI) metal ions in the field of industrial wastewater treatment, including application of magnetite nano-particles **[3]** and different types of ferrites such as nickel, cobalt, manganese, and magnesium ferrites **[2]** for the removal of Cr (VI) from simulated electroplating wastewater; removal of Cr (VI) and Alizarin Red S (ARS) from aquatic environment using magnetic nano-particles (Fe_3O_4) reformed by polymer **[4]**; application of Fe_3O_4 magnetic nano-particles with functional groups of amines for removal of Cu (II) and Cr (VI) heavy metal ions **[5]**; using manganese ferrite nano-spheres **[6]** and surface-modified manganese ferrite **[7]** to remove Cr (VI) ions from wastewater; treatment of wastewater contaminated by Cr (VI) ions by Fe_3O_4 coated glycine doped polypyrrole magnetic nano-composite **[8]**;

Arsenic and Cr (VI) adsorption from water by ionically modified magnetic nano-materials **[9]**. Moreover, Patel *et al*. **[10]** studied the characterization of barium hexaferrite nano-particles to demonstrate its efficiency for the removal of arsenic from water resources. The results of the adsorption process revealed that 75% of Arsenic heavy metal ions effectively removed by barium hexaferrite nano-adsorbent. Byun *et al*. [**11**] synthesized the thinnest barium ferrite nano-fiber by an organic solvent-free electrospining procedure. The prepared nano-fiber packed into a column evidently removed 12 nm magnetite nano-particles quantitatively. Then, pre-adsorption of arsenic onto magnetite nanoparticles was performed with different initial arsenic concentrations. The results showed that barium hexaferrite nano-fiber could support in removing arsenic with a maximum capacity of 700 mg of magnetic nanoparticles for a 99.9 % recovery. Kara et al. [**12**] revealed the feasibility of using barium ferrite containing metal-chelate microbeads (53-212 μm) for the adsorption of Cr (VI) from aqueous solution. They exhibited the highest Cr (VI) adsorption removal of 32% at pH 2.0 using 50 mg of magnetic nano-particles. So far few work has been reported on the application of nanometric barium hexaferrite magnetic particles and its adsorption kinetics for the removal of heavy metal ions from an aquatic environment. The purpose of this investigation therefore is to obtain an understanding of the adsorption of Cr (VI) on barium hexaferrite nano-adsorbent by studying the influence of synthesis variables and different experimental parameters on the adsorption process. In this regard, among varied methods for preparation of barium hexaferrite nanoparticles, co-precipitation is considered due to simple operation and ease of mass production. Moreover, the adsorption kinetics is investigated using the pseudo first-order and pseudo second-order equations. Thus, by considering the high magnetic properties and high separation capacity of barium hexaferrite nano-particles to effectively remove Cr (VI) metal ions from an aqueous solution, it can be set to become an active adsorbent for the removal of the other heavy metal ions from natural water supplies and industrial wastewater in the environmental protection field.

Experimental

Materials

Ferric chloride ($FeCl_3.6H_2O$) and barium chloride ($BaCl_2.2H_2O$) both with a purity of 99% (Merck) were used as starting materials. Sodium hydroxide (NaOH)with a purity of 97% (Merck) was used as a precipitant for co-precipitation of iron and ferric chlorides solution and deionized water and ethanol (CH_3CH_2OH) with a purity of 96% (Merck) were used as solvents.

Materials synthesis

$FeCl_3.6H_2O$ and $BaCl_2.2H_2O$ with a Fe^{3+}/Ba^{2+} molar ratio of 11 were dissolved in two different solvents of water and ethanol/water mixture with volume ratio of 3:1. The prepared solutions were co-precipitated by adding of NaOH with an OH^-/Cl^- molar ratio of 2 at room temperature to keep pH at 11-12. The co-precipitated samples were washed by deionized water and ethanol for about 5 times and then dried at 80˚C for 18 h. Dried powders derived from two different solvents of water and ethanol/water mixture were calcined at 900 and 700˚C, respectively **[13-14]**. In order to study the effect of mechanical milling as a synthesis variable on the adsorption capacity of barium hexaferrite nano-particles, the prepared powders were also milled in a high energy planetary ball mill with hardened steel vial and balls under air atmosphere for 5 h. The balls to powder weight ratio and spinning speed were adjusted to 20 and 300 r/min, respectively. The samples and processing conditions of the prepared barium hexaferrite powders are summarized in **Table 1**.

Table 1. Description of the prepared samples under different synthesis conditions

Sample	Calcination temperature (˚C)	Solvent	Milling time (h)
S1	900	Water	0
S2	700	Water/ethanol	0
S3	900	Water	5
S4	700	Water/ethanol	5

Characterizations

Samples were characterized in phase composition by X-ray diffraction (XRD) on a Philips PW-1730 X-ray diffractometer using Cu-K_α radiation (λ=1.5405 A°). The average crystallite size of barium hexaferrite phase for non-milled and milled samples were calculated by the Scherrer and Williamson-Hall equations, respectively **[15-16]**. The microstructure of the prepared samples was characterized using a field emission scanning electron microscope (FESEM) CamScan MV2300. The multilateral interoperability programme (MIP) software was used to calculate the average particle sizes of all prepared samples from FESEM images. The average specific surface area S_a of the powders was determined by nitrogen adsorption at 77 K (BEL-Belsorp II instrument) employing the Brunauer–Emmett–Teller (BET) isotherm equation. Magnetic properties were measured using a vibrating sample magnetometer (VSM) under a maximum applied field of 10 kOe at ambient temperature. Adsorption experiments were carried out with a mechanical stirrer at ambient temperature and a shaking rate of 300 r/min. The Cr (VI) solution prepared from potassium dichromate ($K_2Cr_2O_7$) powder with a purity of 99% (Merck), which was touched by $BaFe_{12}O_{19}$ magnetic nano-powders in the mechanical stirrer. Standard acid (0.1 M HNO_3) and base (0.1 M NaOH) solutions were used for pH adjustment. The initial and optional adsorption parameters were pH 7.0, initial Cr (VI) concentration of 480 mg/L, amount of nano-particles of 0.5 g, and a contact time of 8 h according to our previous work **[17]**. In the second step, the initial adsorption parameters were examined using all the prepared samples to set the optimized one. Then, in order for Cr (VI) to be removed at the high level by the optimized sample, adsorption studies obtained from different amount of the optimized sample from 0.5-2 g, initial Cr (VI) concentration from 100-480 mg/L at different pH levels of 3-9 and a contact time of 1 h. After the adsorption process was finished, the nano-adsorbent was separated by an

external magnetic field and the supernatant was collected for metal concentration measurements. The concentration of Cr (VI) was measured by an inductively coupled plasma-atomic emission spectrometer (ICP-AMS). Fourier transform infrared spectroscopy (FTIR) spectra of the optimized sample before and after adsorption experiment in the IR range of 400–4000 cm^{-1} were recorded by Bruker Equinox 55 spectrometer.

Theory

The amount of Cr (VI) or total Cr adsorbed per unit mass of barium hexaferrite was evaluated as eq. 1 **[6]**:

$$q_e = \frac{(C_i - C_f)\,V}{m} \quad (1)$$

where, q_e is the equilibrium adsorption capacity of Cr (VI) (mg/g), C_i is the initial concentration of Cr (VI), C_e is the equilibrium concentration of Cr (VI) (mg/L), V is the volume of the Cr (VI) solution (mL), and m is the amount of adsorbent (mg).

The Cr (VI) removal percentage (R%) was calculated using the following equation **[6]**:

$$R\,\% = \frac{C_i - C_f}{C_i} \times 100 \quad (2)$$

where, C_i and C_f are the initial and final concentrations of Cr (VI).

Pseudo-first-order model (eq. 3) and pseudo-second-order model (eq. 4) were used to fit the experimental data for kinetic studies **[18-19]**.

$$log(q_e - q_t) = logq_e - \frac{k_1 t}{2.303} \quad (3)$$

$$\frac{t}{q_t} = \frac{1}{k_2 q_e^2} + \frac{1}{q_e} \quad (4)$$

where, q_e and q_t is Cr (VI) uptake at equilibrium condition and any time t and k_1 and k_2 are the pseudo-first-order and pseudo-second-order rate constants, respectively.

Results and discussion

Phase analysis

Fig. **1** shows the XRD patterns of the S1, S2, S3 and S4 samples. Analysis of XRD patterns confirms the formation of barium hexaferrite single phase in all four prepared samples. While the calcination temperature of 900°C is the suitable temperature for S1 sample to form pure phase of barium hexaferrite, this temperature decreased to 700°C for S2 sample. It is concluded that using ethanol as a co-solvent significantly lower the formation temperature of single phase of barium hexaferrite **[14]**. By employing mechanical milling, this process not only can produce particulate powders with nanometer size due to the contact surface among particles, but also using ethanol as a co-solvent along with mechanical milling process results in the broaden and softer peaks of single $BaFe_{12}O_{19}$ phase for S4 sample in comparison to the other samples.

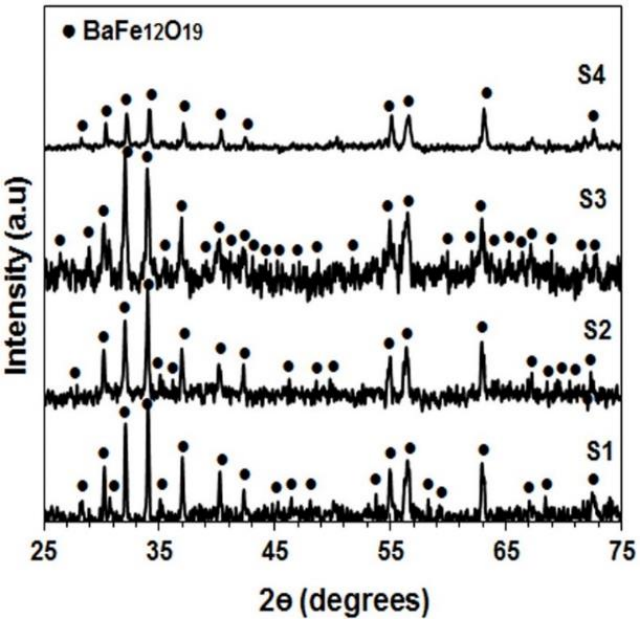

Fig. 1. XRD patterns of S1, S2, S3 and S4 samples.

The mean crystallite sizes of all prepared samples calculated from XRD patterns are shown in **Fig. 2**. It is shown that the mean crystallite sizes of single phase barium hexaferrite for S1, S2, S3 and S4 samples are 57.0, 47.0, 39.3, and 27.0, respectively. It is accepted that the solution environment, the properties of the solvent, and mechanical milling process as synthesis variables can remarkably influence the formation trend of the precursor particles and nucleation and growth of crystals **[14, 20]**.

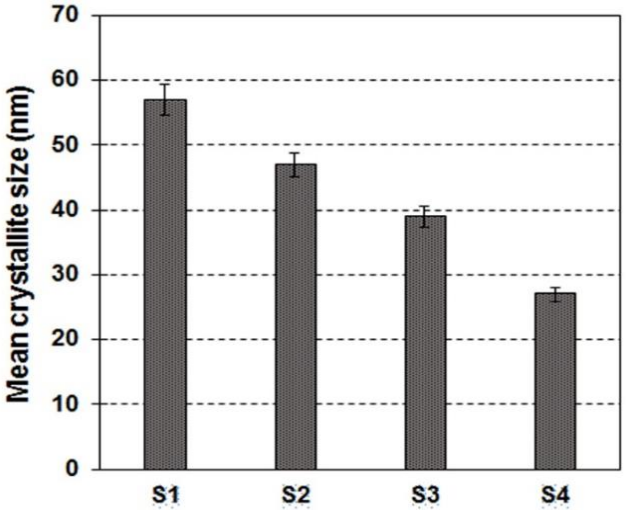

Fig. 2. Calculated mean crystallite sizes of S1, S2, S3 and S4 samples.

Morphological studies

Fig. **3** shows the FESEM images of different samples, on which the effect of solvent and mechanical milling on the powder morphology is reflected. FESEM image in **Fig**. **3** (a) shows that calcination at 900˚C for 1 h for S1 sample is

sufficient enough to form barium hexaferrite nano-particles with a plate-like morphology, which is in good harmony with the XRD results. Also, agglomerates stack in side of each other showing hexagonal-like particles with high magnetic attraction, a characteristic of barium hexaferrite nano-particles obtained by wet chemical methods **[3]**. It seems that morphology was affected by the type of solvent. When the barium hexaferrite powders treated in water as a solvent, they have a preference to form large particles of a hard agglomeration due to the unique property of water molecules to bridge the surface hydroxyl groups of precipitate adjacent small particles **[14]**. On the other hand, by considering ethanol as a co-solvent, particle-particle interaction is prevented and results in softer agglomeration nature with continuous hexagonal structure, which is shown in **Fig**. **3(b)**. It is supported by the fact that ethanol is proposed to the ability to weaken the hydrogen bands between surface hydroxyl groups of neighboring particles and its low surface tension also makes easy the formation of barium hexaferrite phase **[14]**. Moreover, **Fig. 3 (c)** and **(d)** depict the influence of mechanical milling on the morphology of the products. Agglomerated plate-like particles of barium hexaferrite could be observed in both samples. Moreover, some spherical particles are rarely observed besides hexagonal particles. They can be considered as the intermediate phases of particles undetectable by the related XRD patterns.

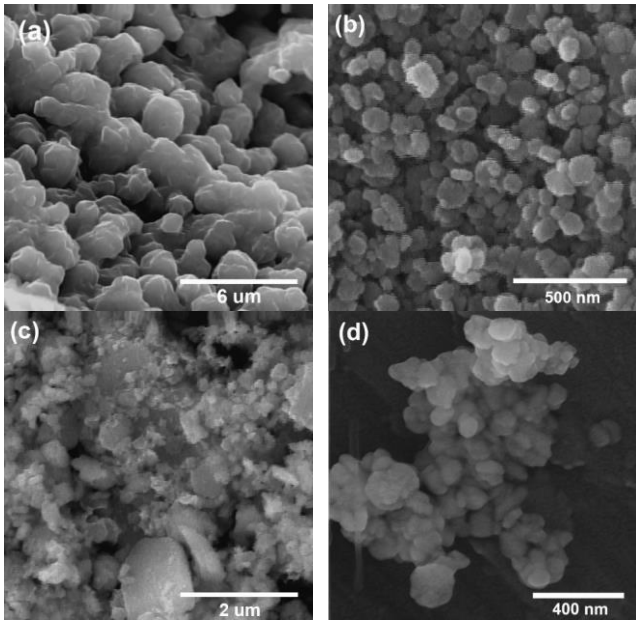

Fig. 3. FESEM images of (a) S1, (b) S2, (c) S3 and (d) S4 samples.

The average particle sizes calculated from FESEM images related to all samples prepared under different synthesis conditions are shown in **Fig**. **4**. It can be observed that the mean particle sizes of S1 and S2 samples are 145 and 90 nm, respectively. It is believed that the variation of the mean particle sizes of the samples is as a function of the calcination temperature **[14]**. Accordingly, low calcination temperature confirms grain refinement. By considering the role of final mechanical milling on S1 and S2 samples, the mean particle sizes decreased from 145 to 118 nm and from 90 to 87 nm for S3 and S4 samples, respectively.

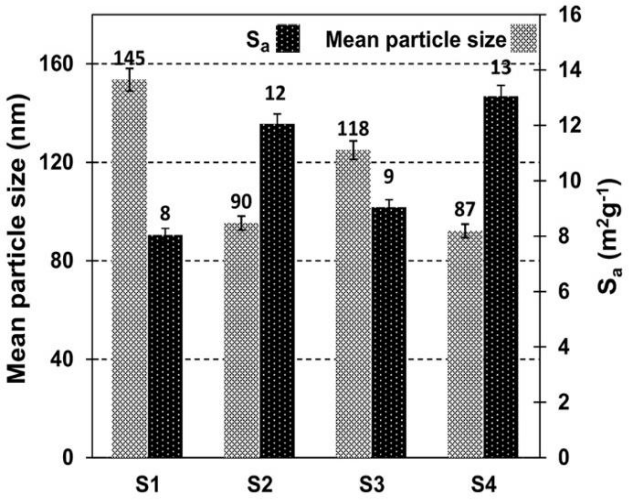

Fig. 4. Calculated average barium hexaferrite particle sizes of S1, S2, S3 and S4 samples.

Also, the calculated S_a by BET method for S1, S2, S3 and S4 samples are shown in **Fig**. **4**. Indeed, higher values of S_a are consistent with lower values of the average barium hexaferrite particle sizes. It can be found that the maximum surface is of 13 m^2/g is related to S4 sample.

Table 2. Description of the magnetic properties of all prepared samples under different synthesis conditions.

Sample	Hc (A/m)	Ms (A.m/kg)
S1	5000	52.9
S2	2600	46.7
S3	5000	34.3
S4	5000	49.6

Magnetic properties studies

The magnetic properties of all prepared samples are shown **Fig. 5**. Also, the magnetic data is summarized in **Table 2**. The saturation magnetization and coercivity of S1 sample were 52.9 emu/g and 5 kOe, respectively. A relatively low value of saturation magnetization might be due to the existence of poorly crystallized phases undetectable by XRD. Also, the reduction in Ms might be due to the decrease in particle size and also in the number of magnetic molecules in a single magnetic domain. This could be supported by the reality that the magnetization of ultrafine particles is smaller than that of the corresponding bulk materials **[21]**. It is evident from the magnetic hysteresis loop of S2 sample that by decreasing calcination temperature from 900 to 700°C, the saturation magnetization decreased from 52.9 to 46.7 emu/g, whilst the coercivity values remained almost constant at 5 kOe. Decreasing of Ms could be due to the decrease in the amount of barium hexaferrite magnetic phase necessary to formed. With considering two important factors on S1 sample: the effect of mechanical milling and decreased particle size, it is clearly seen that saturation magnetization decreased from 52.9 to 34.3 emu/g for S3 sample. Moreover, it is known in barium hexaferrite that the amount of coercivity is intimately related to the nanometric structure and the amount of $BaFe_{12}O_{19}$ magnetic phase **[20]**. The intensive discrepancies between the coercivity values

of S1 (5kOe) and S3 samples (2.6 kOe) might be due to the more crystal defects introduced as a function of mechanical milling applied to S1 sample.

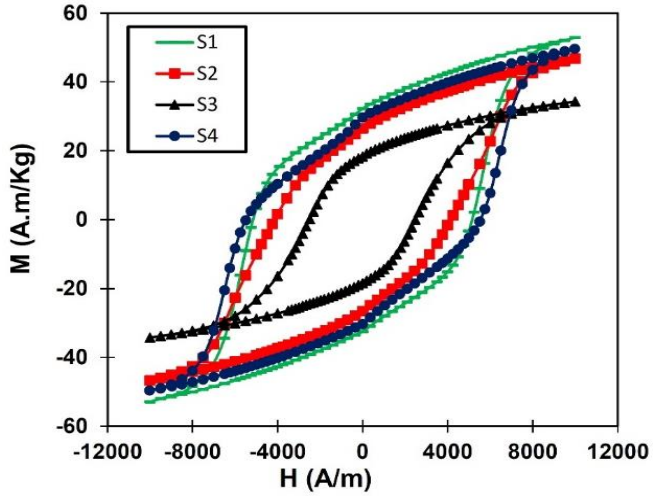

Fig. 5. Room temperature magnetic hysteresis loops of S1, S2, S3 and S4 samples.

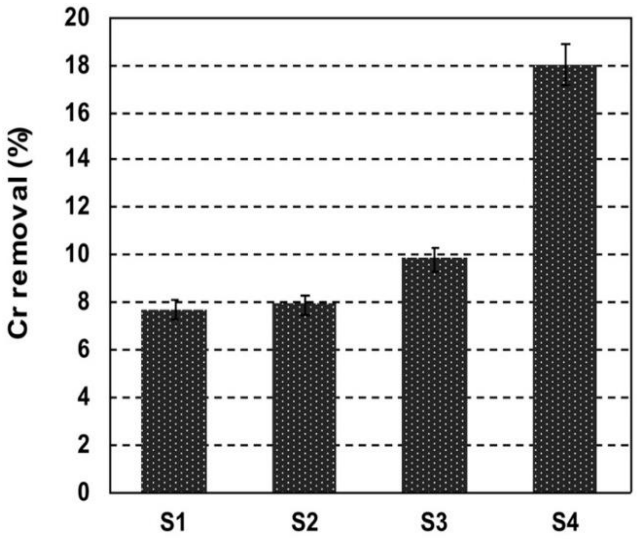

Fig. 6. Cr (VI) removal percentages in a contact time of 8 h under initial adsorption conditions.

Adsorption studies

The adsorption results of Cr (VI) by four produced barium hexaferrite powders include two steps: the first step is to find the optimized sample among four prepared samples under the initial and optional adsorption experiments according to our previous study **[17]**. The results of adsorption tests and percentage of Cr (VI) removal for S1, S2, S3 and S4 samples in a contact time of 8 h have been given in **Fig**. **6**. As **Fig**. **6** shows, the most effective adsorption process of Cr (VI) ions is identified by S4 sample. This result attributes to the fact that finer particles size of barium hexaferrite leads to higher removal efficiency of Cr (VI). It can be determined that the factor of high surface area of S4 sample (13 m^2/g) is more effective for the high removal efficiency of Cr (VI). Therefore, this sample with the high removal percentage of 18% in a contact time of 8 h is considered as an optimized one for which the optimal adsorption parameters have been obtained in the second step.

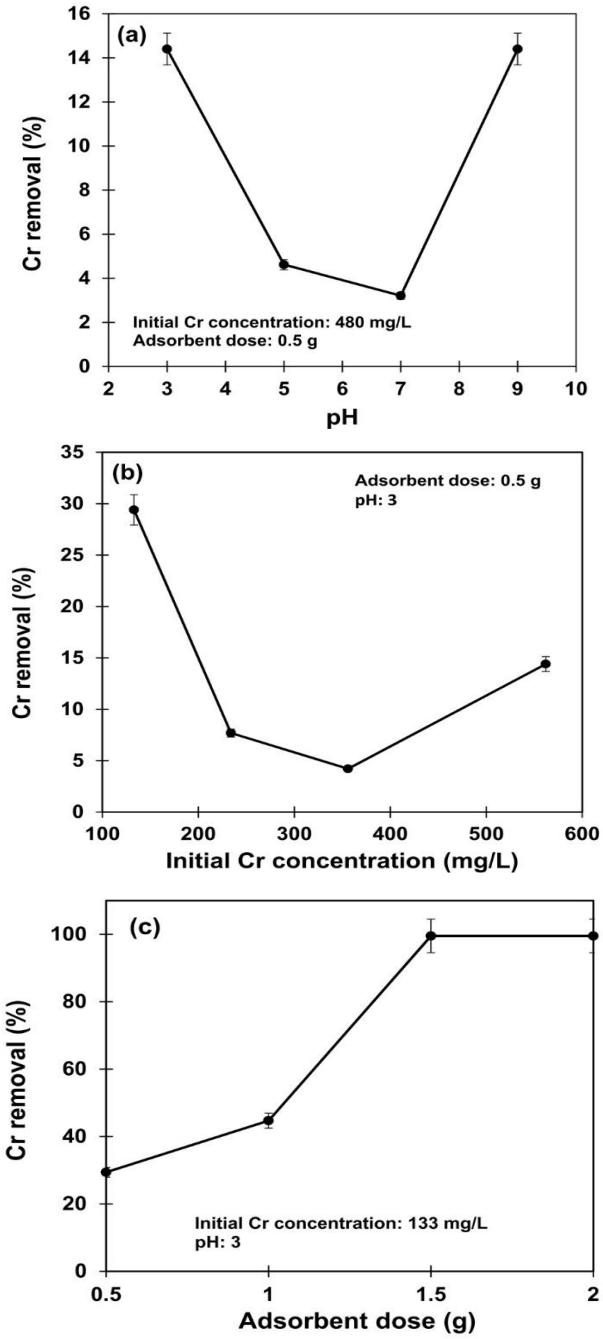

Fig. 7. Comparison of Cr (VI) removal efficiency under different adsorption conditions: (a) pH, (b) Initial Cr (VI) concentration, (c) amount of nano-adsorbent after adsorption process done by the optimized sample (S4).

In the second step, Cr (VI) solution under different adsorption parameters: pH, initial Cr (VI) concentration, and amount of barium hexaferrite nano-particles was touched by S4 sample. This process was resulted in obtaining the optimal adsorption conditions by which the Cr (VI) was significantly removed from solution. **Fig. 7** shows Cr (VI) removal efficiency under different adsorption condition**s**. **Fig. 7 (a)** displays the effect of pH in the range of3-9 on Cr (VI) adsorption using 0.5 g of S4

powder and initial Cr (VI) concentration of 480 mg/L. As it can be seen, the optimal pH for the high removal percentage of Cr (VI) was considered to be 3.0 and 9.0. The adsorption of Cr (VI) metal ions onto the surface of S4 sample as nano-adsorbent is generally affected by pH, since it not only changes the degree of ionization and speciation of the adsorbate during reaction, but also the surface charge of the adsorbent **[10]**. Regarding to the results, the effect of pH for higher removal of Cr (VI) metal ions by this adsorbent can be described as below: the adsorption of Cr (VI) ions depends on the protonation of functional groups on the surface of nano-adsorbent and equally the fraction of any particular species is dependent on Cr (VI) concentration and pH. It has been reported that Cr (VI) ions exist mainly in the form of $HCrO_4^-$ and $Cr_2O_7^{2-}$ in the pH range of 3-6, while CrO_4^{2-} is major Cr (VI) species above pH of 6.0 **[10]**. As the pH $_{zpc}$ of barium hexaferrite nano-particles is 5±0.5 **[22]**. The surface of barium hexaferrite is positively charged below pH 5±0.5, which leads to an electrostatic attraction for the negatively charged Cr (VI) species in the pH range of 3-6. However, as the solution pH increases beyond 6.0, the adsorption surface of the adsorbent is negatively charged, increasing electrostatic repulsion between negatively charged Cr (VI) species and adsorbent particles. Accordingly, due to the higher concentration of $O\bar{H}$ ions present which compete with Cr (VI) species for the adsorption sites, uptake of Cr (VI) ions decreased. Studies by others also showed that the optimum pH for maximum removal Cr (VI) occurred in the acidic pH and by increasing pH up to the base level Cr (VI) removal percentage decreased **[9]**. From the pH study, it was found that efficient outcome of Cr (VI) adsorption with higher removal capacity of 14.4%occurs in the acidic pH of 3.0. Thus, the remaining adsorption experiments are carried out at that pH considered as the optimal one. **Fig. 7 (b)** shows the effect of initial Cr (VI) concentration on chromium adsorption using 0.5 g of S4 powder at optimal pH of 3.0. It is shown that by increasing concentration from 133 to 562 mg/L, removal efficiency of Cr (VI) was reduced from 29.4 to 14.4 percent. This could be supported by the fact that the adsorption reaction is via surface adsorption with limited sites on barium hexaferrite surface available for Cr (VI) ions. Due to the limited total available adsorption sites, it can be concluded that Cr (VI) removal is conversely related to the initial Cr (VI) concentration.[3] In addition, it was also observed that the optimal value of Cr (VI) concentration is 133 mg/L, in which the most efficient removal percentage of 29.4% was resulted. Therefore, to obtain the optimal values of the other parameters, the experiments went on using 133 mg/L concentration of Cr (VI). **Fig. 7 (c)**, shows the effect of adsorbent dose on Cr (VI) adsorption with optimal pH of 3.0 and initial Cr (VI) concentration of 133 mg/L. It can be seen that higher amount of barium hexaferrite nano-particles directs to higher removal percentage. It is readily understood that due to the increase in the number of active sites available for adsorption, the removal efficiency of Cr (VI) increased. Previous studies have also emphasized this point **[10]**. Moreover, the results of adsorption reaction using 1.5 and 2 g nano-particles were found to be almost the same. So, the optimal value of the adsorbent dose for the removal of Cr (VI) is considered 1.5 g. Thus, the second step of adsorption experiment leading to the maximum removal efficiency of 99.5% using 5 h milled barium hexaferrite nano-powder by controlling the optimal adsorption conditions: pH 3.0, Cr (VI) concentration 133 mg/L, volume of solution 150 mL, amount of nano-particles 1.5 g, contact time 1 h, temperature 25˚C, and shaking rate 300 r/min is done.

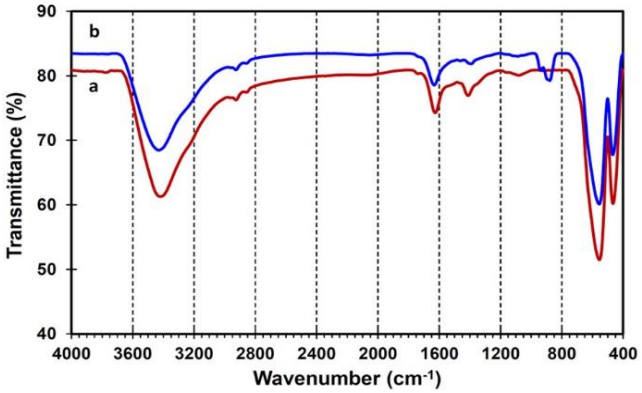

Fig. 8. FTIR spectra of the optimized sample: (a) before adsorption (b) after adsorption.

FTIR analysis results of the optimized sample

To investigate the electrostatic reaction done on the optimized sample to adsorb Cr (VI) ions from aqueous solution, the chemical bands and possible phase compositions existing in the optimized sample before and after adsorption experiment were demonstrated by FTIR analysis. FTIR spectrum of the optimized sample before and after adsorption method in the range of 400–4000 cm^{-1} is presented in **Fig. 8 (a)** and **(b)**, respectively. As can be seen, although the positions of their main peaks are almost consistent with each other, two curves seem different. The broad bands centered at 3420 and 3431 cm^{-1} for the optimized sample before and after adsorption procedure, respectively are due to the O–H stretching. The absorption bonds around 3200–3500 cm^{-1} relate to the O–H stretching mode, where freely vibrating OH groups and hydrogen-bonded OH groups are obvious **[23]**. The spectra display an O–H bending band of the H_2O molecules chemically adsorbed to the magnetic particle surface around 1620 and 1633 cm^{-1}.These peaks are assigned to the H–O–H bending vibration **[14]**. The characteristic of this peak for the optimized sample after adsorption may be due to more water present either as absorbed water or water of hydration. The absorption bands at 1412 and 1396 cm^{-1} resulted from the carbonate groups **[14]**. Increasing the distinctive band of the $BaCO_3$ at 1412 cm^{-1} before the adsorption reaction confirms the more amounts of this composition. Also, the presence of $BaCO_3$ in these samples, were not detected, as observed by others **[24]**, indicating that the adopted ceramic method (milling and calcination) was efficient to consume fully the starting reagents. Also, the peaks in the ranges 420–450 and 540–600 cm^{-1} can be attributed to the stretching vibration of the metal–oxygen bond indicating the formation of a hexaferrite structure including octahedral and tetrahedral sites, respectively **[23]**. It was observed that two new peaks appeared at 879 and 942 cm^{-1} for the optimized sample after the adsorption

process, which are seen in **Fig. 8 (b)**. The main difference of the samples before and after adsorption are attributed to these new peaks, which may define the occurrence of the electrostatic reaction done between the Cr (VI) metal ions in the solution and the surface of barium hexaferrite nano-adsorbent. The chemistry of aqueous chromate solutions has been studied widely by different techniques. From these studies, the following chemical equilibria were suggested **[25]**:

$$CrO_4^{2-} + H^+ \leftrightarrow HCrO_4^- \quad (5)$$
$$2CrO_4^{2-} + 2H^+ \leftrightarrow Cr_2O_7^{2-} + H_2O \quad (6)$$
$$2HCrO_4^- \leftrightarrow Cr_2O_7^{2-} + H_2O \quad (7)$$

The above chemical equilibria as well as the Cr (VI) concentration and pH describe which specific Cr (VI) species be in the majority in solution. In basic solutions above pH 6, the major Cr (VI) species is CrO_4^{2-}; in pH range of 3-6 both $HCrO_4^-$ and $Cr_2O_7^{2-}$ are dominant chromate species in solution. It is reported that the stretching bands between 846 to 860 cm^{-1} and 860-870 cm^{-1} are assigned to the CrO_4^{2-} ions in the neat chromates of barium and strontium and to the matrix-isolated CrO_4^{2-} guest ions, respectively **[26]**. While, the symmetric stretch of the dimeric $Cr_2O_7^{2-}$ species performs at the high wave number side of the 870 cm^{-1} band; that is, 904-954cm^{-1} **[27]**. Besides, it is reported that the most intense peak of the spectrum of $HCrO_4^-$ was estimated to be in the region of 880 cm^{-1} and would be strongly polarized **[28]**. According to this fact that the chromium solution for the optimized sample was prepared at pH 3.0, the main chromate species in the solution is $Cr_2O_7^{2-}$. Therefore, the appeared peaks for the optimized sample after adsorption at 879 cm^{-1} and 942 cm^{-1} correspond to the symmetric stretch of CrO_2 and CrO_3 groups of the ionic $HCrO_4^-$ and the dimeric $Cr_2O_7^{2-}$ species, respectively. It was revealed that the Cr (VI) ions indicated a stretching bands of Cr-oxygen by which Cr (VI) ions effectively adsorb on the surface of barium hexaferrite nano-particles. It is concluded that the barium hexaferrite magnetic nano-adsorbent showed a quite good capability for the rapid and efficient adsorption of chromium metal anions from aqueous solution, which was confirmed by FTIR results.

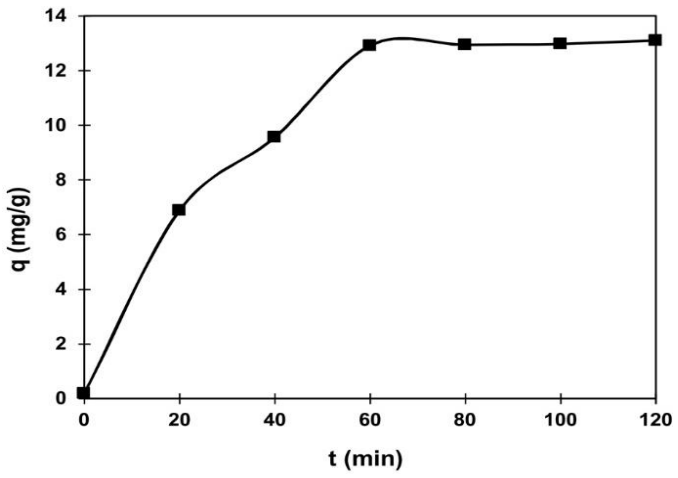

Fig. 9. Effect of contact time on the removal of Cr (VI) by the optimized sample (pH: 3.0, Concentration: 133 mg/L, Nano-adsorbent: 1.5 g, Temperature: 25ºC).

Effect of contact time and adsorption kinetics

Adsorption kinetics is one of the important characteristics that explain the efficiency of adsorption. The Cr (VI) uptake as a function of contact time onto the optimized sample at an initial Cr (VI) concentration of 133 mg/L, pH 3.0, the amount of nano-adsorbent 1.5 g, and 25°C is presented in **Fig. 9**. It is found that the adsorption rate was fast at the initial time and reaches the equilibrium within 60 min. The rapid adsorption of the optimized sample is because of the high surface area and more active sites of the adsorbent. At equilibrium, the adsorption capacity of Cr (VI) was found to be 13.25 mg/g. To study the adsorption rate and rate controlling step, two commonly kinetic models: pseudo-first-order and pseudo-second-order were applied.

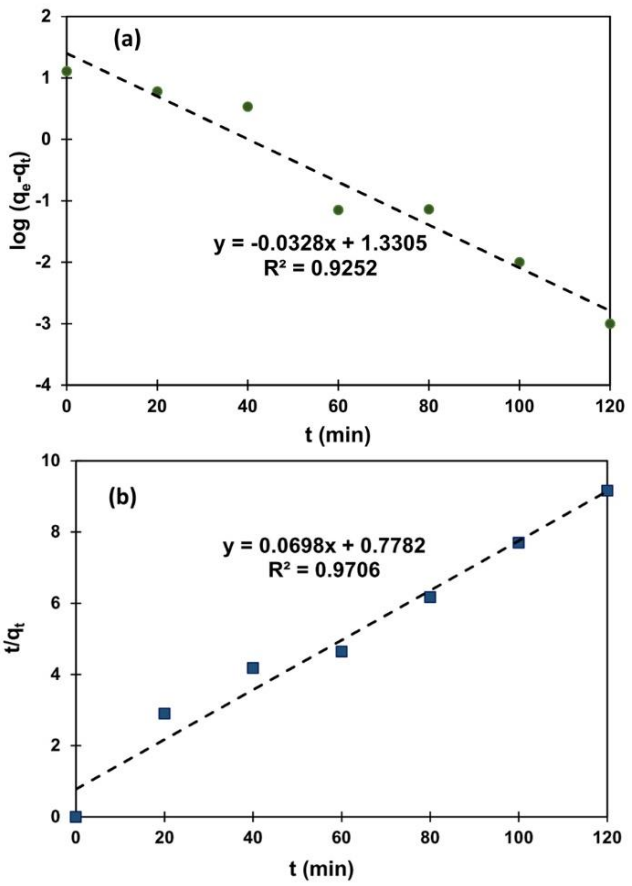

Fig. 10. Linear plot of kinetic models for the adsorption of Cr (VI) ions: (a) pseudo-first-order (b) pseudo-second-order.

The plots of the two kinetic models are shown in **Fig. 10 (a)** and **(b)**. As can be seen, pseudo-second-order describes the adsorption kinetics better than pseudo-first-order model due to higher values of correlation coefficients (R^2). The calculated equilibrium adsorption capacity and constant rate values for Cr (VI) adsorption using pseudo-second-order rate equation were 14.3 mg/g and 0.0063g mg^{-1} min^{-1}, respectively. In contrast, the calculated equilibrium adsorption capacity and constant rate values for Cr (VI) adsorption using pseudo-firs-order rate equation were 21.4 mg/g and 0.075 min^{-1}, respectively. From the obtained results, it is concluded that pseudo-second-order model was effectively adapted to the

experimental data which helps describe the possible adsorption mechanisms.

Conclusion

Barium heaxaferrite nano-particles have been successfully produced by co-precipitation method. The crystallite sizes of different magnetic nano-powders found to be in the range of 27-57 nm. FESEM images of the optimized sample (S4) revealed fairly hexagonal morphology of nano-particles with a mean particle size of 87 nm with the high surface area of 13 m^2/g, and relatively high magnetic properties (Hc: 5kOe and Ms: 49.6 emu/g) was also obtained. It was conclusively obvious from bath adsorption studies that the use of all types of nano-scale barium hexaferrite for Cr (VI) removal was technically possible, environmentally-friendly and economically attractive for the treatment of Cr-contaminated solutions. By comparison of adsorption results among all types of the prepared samples, the optimized barium hexaferrite nano-particles stands out for having the highest Cr (VI) removal efficiency of 99.5% at the optimized adsorption conditions: pH 3.0, initial chromium concentration 133 mg/L, amount of nano-particles 1.5 g at the shortest adsorption time of 1 h. FTIR analysis revealed that the Cr (VI) ions indicated a stretching bands of Cr-oxygen by which Cr (VI) ions effectively adsorb on the surface of barium hexaferrite nano-particles Also, the adsorption data fitted the pseudo-second-order kinetic model well. So, the present study succeeded in producing the most potential magnetic nano-adsorbent for the fast removal of Cr (VI) metal ions from polluted aqueous solutions, which can be applicable for the removal of the other heavy metal ions from industrial wastewaters.

Acknowledgements

The financial supports of this work by the University of Tehran (grant number 30052/1/01) and Iran Nanotechnology Initiative Council are gratefully acknowledged.

Reference

1. Shen, H.; Chen, J.; Dai, H.; Wang, L.; Hu, M. *J. Ind. Eng. Chem. Res.*, **2013**, *52*, 12723. **DOI:** 10.1021/ie4010805
2. Hu, J.; Lo, I.M.C.; Chen, G. *J. Sep. Purif. Technol*., **2007**, *56*, 249. **DOI:** 10.1016/j.seppur.2007.02.009
3. Amin, M. M.; Khodabakhshi, A.; Mozafari, M.; Bina, B.; Kheiri, S. *J. Environ. Eng. Manag*., **2010**, *9*, 921. **DOI:** http://omicron.ch.tuiasi.ro/EEMJ
4. Hanif, S.; Shahzad, A. *J. Nanopart. Res*., **2014**, *16*, 2429. **DOI:** 10.1007/s11051-014-2429-8
5. Haung, S. H.; Chen, D. H.; *J. Hazard. Mater*., **2008**, *163***,** 174. **DOI:** 10.1016/j.jhazmat.2008.06.075
6. Yang, L.X.; Wang, F.; Meng, Y.F.; Tang, Q.H.; Liu, Z.Q. *J. Nano. Mat.*, **2013**. **DOI:** 10.1155/2013/293464
7. Hu, J.; Lo, I.M.C.; Chen, G. *Langmuir*. **2005**, *21*, 1173. **DOI:** 10.1021/la051076h
8. Ballav, N.; Choi, H. J.; Mishra, S.B.; Maity, A. *J. Ind. End. Chem*., **2014**, *20*, 4085. **DOI:** 10.1016/j.jiec.2014.01.007
9. Badruddoza, A.Z. M.; Shawon, Z.B.Z.; Rahman, M.T.; Hao, K. W.; Hidajat, K.; Uddin, M. S. *J. Chem. Eng.*, **2013**, *225*, 607. **DOI:** 10.1016/j.cej.2013.03.114
10. Patel, H. A.; Byun, J.; Yavuz, C. T. *J. Nanopart. Res*., **2012**, *14*, 881. **DOI:** 10.1007/s11051-012-0881-x
11. Byun, J.; Patel, H.A.; Yavuz, C.T. *J. Nanopart. Res*., **2014**, *16*, 2787. **DOI:** 10.1007/s11051-014-2787-2
12. Kara, A.; Demirbel, E.; Sozeri, H.; Kucuk. I.; Ovalioglu, H. *J. Biol. Chem.*, **2014**, *42*, 299. **DOI:** http://www.hjbc.hacettepe.edu.tr/journal/volume-42/issue-3/index.html
13. Montazeri-pour, M.; Ataie, A.; Nikkhah-Moshaie, R. J. *IEEE. Trans. Magn.*, **2008**, *44***,** 4239. **DOI:** 10.1109/TMAG.2008.2001811
14. Montazeri-pour, M.; Ataie, A. *J. Mater. Sci. Technol*., **2009**, *25*, 465. **DOI:** http://www.jmst.org/EN/Y2009/V25/I04/465
15. Cullity, B.D. (2nd Eds.); Elements of X-ray Diffraction; *Mass: Addison-Wesley*, **1978**. **DOI:** http://dx.doi.org/10.1119/1.1934486
16. Williamson, G.; Hall, W. *J. Acta. Metall*., **1953**, *1*, 22. **DOI:** 10.1016/0001-6160 (53) 90006-6
17. Mohammadi, A.; Ataie, A.; Sheibani, S. *Int. J. Chem. Environ. Eng*., **2015**, 6, 158.
18. Lagergren, S. *Ksven Vetenskapsakad Handl*. **1898**, 24, 1.
19. Ho, Y.S.; Mckay, G. *Trans. Ichem. E*., **1998**, *76*, 332. **DOI:** 10.1205/095758298529696
20. Hodaei, A.; Ataie, A.; Mostafavi, E.; *J. Alloy. Compd*., **2015**, *640*, 162. **DOI:** 10.1016/j.jallcom.2015.03.230
21. Haneda, K.; Miyakawa, C.H.; Kojima, H. J. Am. Ceram. Soc., **1974**, *57*, 354. **DOI:** 10.1111/j.1151-2916.1974.tb10921.x
22. Kaczmarek, W.A.; Radlinska, E.Z.; Ninham, B.W. *J. Mater. Chem. Phys.*, **1993**, *35*, 31. **DOI:** 10.1016/0254-0584(93)90172-I
23. Najafabadi, A.H.; Mozaffarinia, R.; Ghasemi, A.; J. Supercond. Nov. Magn. **2015**. **DOI:** 10.1007/s10948-015-3119-1
24. Garcia, R.M.; Ruiz, E.R.; Rams, *E.E. Mater. Lett*. **2001**, *50*, 183. **DOI**: 10.1016/S0167-577x (01) 00222-1
25. Cies´lak-Golonka, M. Polyhedron. **1995**, *15*, 3667. **DOI:** 10.1016/0277-5387 (96) 00222-1
26. Stoilova, D.; Georgiev, M.; Marinova, D. *J. Mol. Struct*. **2005**, *738*, 211. **DOI**: 10.1016/j.molstruc.2004.12.016
27. Chua, Y. T.; Stair, P.C.; Wachs, I.E. *J. Phys. Chem. B.* **2001**, *105***,** 8600. **DOI**: 10.1021/jp011366g
28. Michel, G.; Machiroux, R. *J. Raman. Spectrosc*. **1983**, *14*, 22. **DOI:** 10.1002/jrs.1250140107

